

Research Article

Prioritization of Susceptible Watershed to Sediment Yield and Evaluation of Best Management Practice: A Case Study of Awata River, Southern Ethiopia

Temesgen Kefay,¹ Tolera Abdisa,² and Bekan Chelkeba Tumsa ²

¹School of Hydraulic and Water Resources Engineering, Dilla University, Dilla, Ethiopia

²Faculty of Civil and Environmental Engineering, Jimma University, Jimma, Oromia, Ethiopia

Correspondence should be addressed to Bekan Chelkeba Tumsa; bekanchelkeba@gmail.com

Received 15 March 2022; Accepted 8 April 2022; Published 22 April 2022

Academic Editor: Balram Ambade

Copyright © 2022 Temesgen Kefay et al. This is an open access article distributed under the Creative Commons Attribution License, which permits unrestricted use, distribution, and reproduction in any medium, provided the original work is properly cited.

Soil erosion is currently a global problem that causes land degradation and long-lasting challenges in Ethiopia. Sediment yield is influenced by the watershed characteristics such as land cover, soil class, and slope, which are considered the drivers of soil erosion in the basin. The middle Awata watershed is highly susceptible to soil erosion due to its topographical features. This study is therefore aimed at estimating sediment yield, examining its spatial distribution, and evaluating the selected Best Management Practices (BMPs) to reduce soil erosion-prone areas at downstream. The model simulation was done by dividing the total watershed area of 1912 km² into 37 subbasins and 294 hydrologic response units (HRUs) for 31 years (1988–2018). The model's uncertainty evaluation was carried out on monthly basis using the Sequential Uncertainty Fitting (SUFI-2) algorithm. The performance of the model was evaluated by statistical parameters that gave $R^2 = 0.76$, $NSE = 0.75$, $RSR = 0.51$, and $PBIAS = 5.6\%$ for calibration and $R^2 = 0.75$, $NSE = 0.74$, $RSR = 0.51$, and $PBIAS = 2.7\%$ for validation of streamflow. Meanwhile, sediment yield in the watershed was also simulated with $R^2 = 0.69$, $NSE = 0.66$, $RSR = 0.58$, and $PBIAS = 3.7\%$ for calibration and $R^2 = 0.67$, $NSE = 0.65$, $RSR = 0.61$, and $PBIAS = 5.6\%$ for validation of sediment distribution. The simulated annual average sediment yield was 34.543×10^3 ton/year at the outlet of the middle Awata watershed. The developed spatial distribution of sediment yield identified the first twelve upstream subwatersheds as being soil erosion-prone areas. Following an evaluation of the four selected BMPs, it was determined that parallel terracing is the most recommended method for soil erosion reduction option in all critical subbasins found in the watershed.

1. Introduction

A comprehensive understanding of hydrological processes in the watershed is the first step for successful water management and environmental restoration [1]. Variability in climate, changes in land cover (deforestation), and overgrazing have all contributed to land degradation and soil erosion in many African watershed regions [2]. As far as erosion is a worldwide natural process causing land degradation due to the removal of soil in valleys and mountainous and highland areas, it causes sedimentation in lowland floodplains [3]. The accumulated soil in river reaches, reservoirs, or lakes is progressively causing an

increase in the bed level of structures [4]. According to [5, 6], the cumulative incoming sediment load deposited in natural lakes with no outlets results in a lifetime reduction of any downstream water resource projects and even natural lakes. In most parts of the world, soil erosion has been described as the most serious threat to land loss and crop yield [7, 8]. Because of poor landuse practices, ineffective management systems, and a lack of appropriate soil conservation measures, Ethiopia has high rates of soil erosion and land degradation [9, 10]. Soil loss is one of the current critical problems throughout Ethiopia, and its occurrence is mostly in highland areas due to erosive rains, steep slopes, and undulating topography [11]. By detaching soil particles,

climate (precipitation), catchment properties (soil type, topography, and land use/cover), and drainage properties (surface runoff) typically influence sediment yield [12, 13]. These sediments result in a reduction of soil productivity and reservoir capacity. The system of sediment modelling is the simulation of a watershed's response in terms of sediment yield to those influencing factors [14]. Therefore, sediment yield is a useful indicator of land degradation, intensity, and patterns, as well as a reflection of a watershed's characteristics [15]. As a result, sediment yield estimation is needed because it affects reservoir capability, sediment transport to the lake and stream, water quality and quantity, stream habitat, channel morphology, and ecosystem [16]. Sedimentation is a dangerous and destructive obstacle for water resources' planning projects unless the upstream watersheds are handled with effective protective management strategies [17, 18]. Because of the spatial and temporal heterogeneity in soil properties, vegetation, and landuse practices, the hydrologic process is a complex system that exposes the catchments to sedimentation [19]. As a result, mathematical models and geospatial analysis tools are required for studying hydrological processes and hydrological responses to sediment delivery. Furthermore, sediment load modelling provides important planning tools that can be used in land and water resource management by protecting streams, reservoirs, and dams from damage by sedimentation [20].

The SWAT model has proven to be an extremely adaptable method for investigating a wide range of hydrologic processes, sediment yields, and water quality modelling [21]. For example, Ayana et al. [22] applied the SWAT model to the simulation of sediment yield in the Fincha watershed with a total area of 3251 km², and the result was quite acceptable. They also used the model to estimate runoff and sediment yield in the Katar watershed, with a catchment area of 3327 km², in the Rift Valley Lake basin of Ethiopia, and this resulted in successful calibration and validation [23]. This study has been initiated to estimate the sediment yields, identify the critical source area of soil erosion, and map its spatial variability using the SWAT model. Gold mining and agricultural activities are conducted at downstream of the river. The topographic feature is steep and longer slopes with no effective protective measures have been made in the watershed to reduce soil erosion. Sedimentation in the lower reaches of the watershed has caused stream channels to become clogged with sediment which resulted in an increase of bank erosion, meandering, and flooding risk. Furthermore, the study's main objectives were to estimate the rate of annual average sediment inflow to the outlet, map the spatial variability of sediment, identify the most erodible subwatersheds based on their sediment delivery, and evaluate the best management practises (BMPs) for the reduction of sediment yield in the catchment. Sedimentation in the lower reaches of the Awata watershed has caused stream channels to become clogged with sediment, which has resulted in an increase of bank erosion, meandering, and flooding risk. If not properly assessed, indeed, it would highly affect any water resources' project available in this watershed region.

2. Materials and Methods

2.1. Description of the Research Area. The study area, the middle Awata watershed (Figure 1), is a tributary of the Dawa River with a drainage area of 1912 km², located in the northwestern part of the Ganale-Dawa River basin. Geographically, it lies between coordinates of 5°43' to 6°30'N latitude and 38°24' to 39°04'E longitude with an altitude range between 1601 and 3037 m.a.s.l. The study area has been chosen as it is one of the major tributaries in the Ganale-Dawa basin that is highly subjected to the problem of soil erosion and sedimentation in the downstream parts of the river.

2.2. Topography. From DEM data analysis, the middle Awata watershed consists of a complex landscape with various topographical features: flat to mountainous, plains, dissected hills, plateaus, and mountains, as well as valleys and gorges. The upper reaches of the basin are plateau and mountainous, while the middle region is steep and hilly, and the lower basin is flat with a broad meandering river shape. The northern parts of the watershed are covered by basaltic flows and are deeply dissected by the erosive activities of the surrounding rivers [24]. In general, the area's slope is characterized by varying from gentle at the outlet and northern parts to steeper through the middle of the watershed, so that high sediment accumulation possibilities are created over both the upper and lower portions of the watershed.

2.3. Weather Condition. The rainfall pattern of the study area, as indicated in Figure 2, is the bimodal type, which divides the year into two main rainy seasons, namely, spring (April to May) and autumn moderate rain (August to October). The north and northwestern portions of the watershed experience high rainfall and low temperatures, while the lowland areas (southeastern part) experience high temperatures and low rainfall. The mean monthly rainfall of the watershed varies from 25.66 mm to 223.76 mm, and the annual rainfall varies from 1042.27 mm to 1687.71 mm. The monthly average maximum and minimum temperatures of the middle Awata watershed were 25.31°C and 11.34°C, respectively.

2.4. Meteorological, Sedimentary, and Hydrological Data. This study used both spatial and time-series data. The study in this watershed used spatial data such as DEM, soil, and Landsat images for spatial analysis with ArcGIS. Meteorological data for 31 years (1988–2018), such as precipitation, temperature, sunshine hours, relative humidity, and wind speed from six stations found in the catchment, as well as hydrological data such as streamflow for 24 years (1990–2013) and sediment data, were collected by the Ethiopian meteorological agency and the Ministry of Water, Irrigation, and Electricity, respectively; these data were used to predict streamflow and calibrate sediment. Weather stations found in the catchments with their locations are

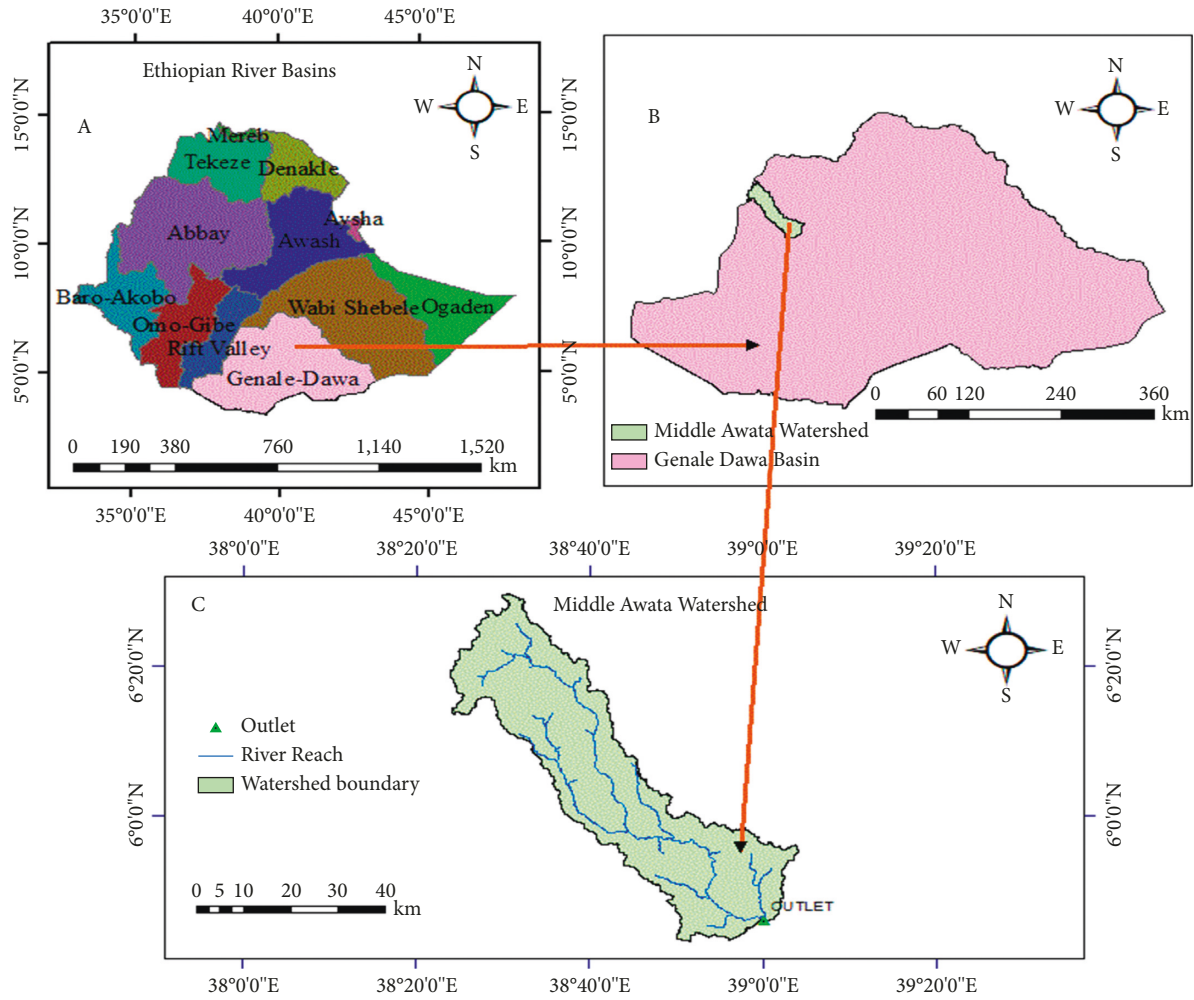


FIGURE 1: Location and map of the study area.

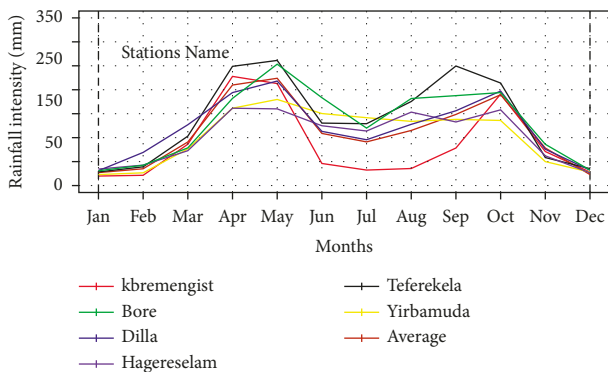


FIGURE 2: Monthly rainfall pattern at each station in the Awata watershed.

depicted in Table 1. A DEM with a 12.5 m × 12.5 m resolution for the study area was downloaded from the Alaska Satellite Facility (<https://asf.alaska.edu>) and used to analyse the drainage patterns of the watershed terrain. The middle Awata watershed had a streamflow gauging station near Oddo-Shakiso located at its outlet as shown in Figure 3. The catchment river discharge depends on seasonal rainfall

variability. The river in the watershed is flowing from the northwestern part towards southeastern direction (outlet) and join Dawa River which is the tributary of Ganale River. The river discharge increases proportionally with the mean precipitation through the two seasons of April to May and August to October. The long-term mean monthly discharge recorded at Awata station was 10.57 m³/s–41.32 m³/s, and the mean annual flow at the station was recorded at around 817.68 million m³/annum.

Rainfall and runoff provide the essential energy input needed to drive erosion processes. The watershed soil erosion and sediment yield are directly proportional to runoff which in turn is directly influenced by the meteorological data. The runoff and sediment yield increase proportionally with the mean precipitation through two seasons of April to May and August to October. As a result, rainfall has been established as the primary source of soil erosion. Other climate characteristics affect soil erosion indirectly. In monsoon, the big seasonal winds blow from southwest bringing heavy rainfall to the area, and the two rainy seasons can be considered as monsoon period. In premonsoon and postmonsoon, there may be less sediment yield due to small sediment detachment and transporting force such as rainfall

TABLE 1: Location of the weather stations and availability of weather data.

No.	Station	Lat	Long	Ele (m)	Weather data elements					
					PCP	T-max	T-min	SSH	WND	HMD
1	Kibremengist	5.87	38.97	1680	✓	✓	✓	✓	✓	✓
2	Teferekella	6.05	38.60	1870	✓	✓	✓	NA	NA	NA
3	Yirbamuda	6.21	38.71	2569	✓	✓	✓	NA	NA	NA
4	Bore	6.35	38.62	2712	✓	✓	✓	NA	NA	NA
5	Hagere Selam	6.49	38.52	2809	✓	✓	✓	NA	NA	NA
6	Dilla	6.37	38.40	2679	✓	✓	✓	NA	NA	NA

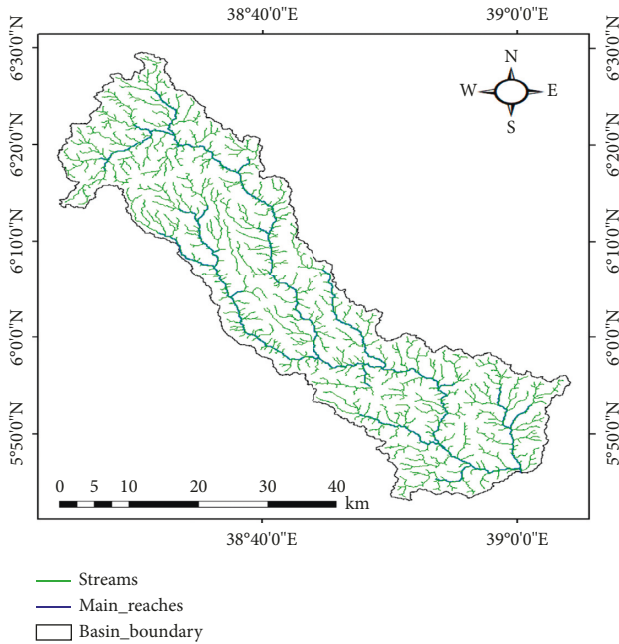


FIGURE 3: Streamflow network of the middle Awata watershed.

and wind. In general, monsoon period may result in the generation of higher sediment than premonsoon and postmonsoon due to high wind blow resulting in heavy rainfall which is directly related to runoff and sediment yield.

2.5. Classification of Soils. The nature and characteristics of underlying soils determine how a river basin reacts to rainfall events and the susceptibility of a watershed to erosion. For different layers of each soil type, the SWAT model requires different soil types and physiochemical parameters such as soil texture, available water content, hydraulic conductivity, bulk density, and organic carbon content [25]. The study area is covered by five dominant soil types as listed in Table 2.

2.6. Land Use and Land Cover. One of the main factors affecting surface erosion, surface runoff, and evapotranspiration of a given watershed is its land use and land cover features [22]. For this study, multispectral satellite images (Landsat-8 OLI/TIRS-2018) of the Awata River watershed were downloaded from the Earth Explorer website for land use and land cover classification. Hence, on this basis, six

TABLE 2: Dominant soil types of the study area.

S. no.	Soil type	Area (km ²)	% of coverage
1	Chromic luvisols	701.07	36.67
2	Eutric leptosols	19.10	0.999
3	Eutric vertisols	316.47	16.55
4	Humic nitisols	754.80	39.48
5	Lithic leptosols	120.32	6.29

different types of land use land cover have been classified as shown in Table 3 using the ERDAS Imagine classifier.

2.6.1. Image Classification and Accuracy Assessment. The supervised classification method was used in this research, which is the most popular sort of classification technique. It automatically categories all pixels with comparable spectral values into land cover classes, as shown in Figure 4. The landuse land cover classification by the supervised method acquires control points collected from the study area to determine the spectral signature of recognized features. About 300 user-defined ground truth points were collected from the image and were classified into six classes by ERDAS software as indicated in Figure 5. As presented in Table 4, accuracy assessment is a crucial step in the final stage of the image classification process. The target of the accuracy evaluation was to assess how well pixels were sampled into the actual land cover classes.

$$\text{Overall accuracy} = \frac{\text{number of points correctly classified}}{\text{total number of points classified}} \quad (1)$$

The kappa coefficient (K) represents an agreement between classified land cover classes, and the observed land cover/use should lie between 0 and 1, where 0 represents weak agreement and 1 represents strong agreement.

$$\text{Kappa (K)} = \frac{Po - Pe}{1 - Pe} \quad (2)$$

Accuracy is the distance between the actual geographic locations of an object compared to the position of the object in the mapped or classified image. Overall accuracy is essentially telling us out of all of the reference ground sites what proportion of images were mapped correctly.

TABLE 3: Types of land use and land cover in the middle Awata watershed (2018).

S. no.	LULC classes	Area (km ²)	% of coverage
1	Shrubland	763.62	39.94
2	Forest land	204.48	10.70
3	Waterbodies	24.08	1.26
4	Grassland	137.87	7.21
5	Built-up area	66.64	3.49
6	Agriculture	715.20	37.41

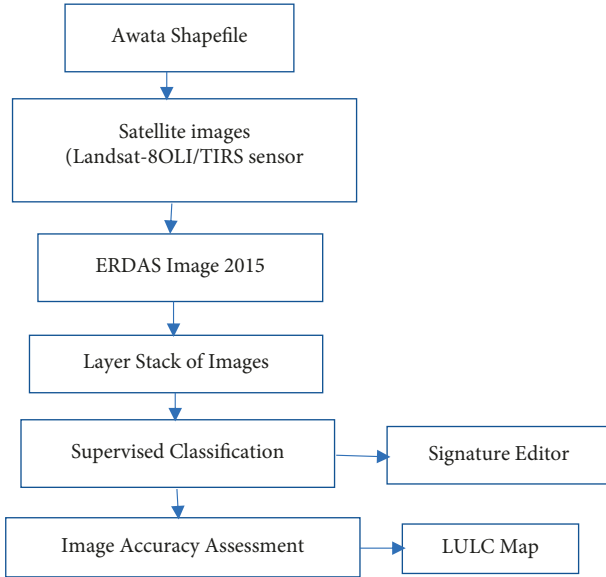


FIGURE 4: Land use land cover image classification diagram.

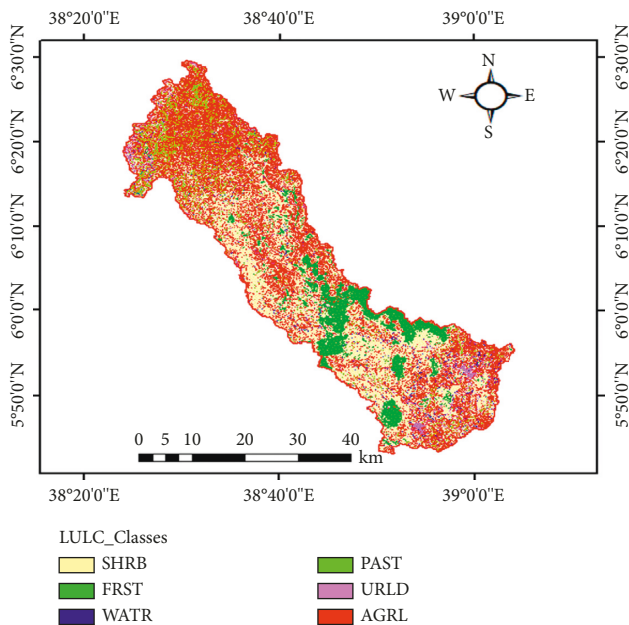


FIGURE 5: Supervised classification of land use land cover map of the middle Awata watershed.

2.7. Methods

2.7.1. *The Approach Based on Sediment Yield and Streamflow.* The SWAT model divides the hydrology of a watershed into the routing phases of the hydrologic cycle. These two stages are largely contained by land and water. The amount of water, sediment, nutrients, and pesticide loadings into the main channel are all controlled by the land phase of the hydrologic cycle. Water, sediment, nutrients, and pesticides are transported via the channel to the subbasin during the routing phase of the hydrologic cycle. These hydrological cycles are simulated by SWAT by referring to the water balance equation indicated by the following equation:

$$SW_t = SW_0 + \sum_{i=1}^t (R_{day} - Q_{sur} - E_a - W_{seep} - Q_{gw}), \quad (3)$$

where SW_t represents soil water content (mm), SW_0 represents soil water content on day i (mm), t represents time (days), R_{day} represents precipitation on day i (mm), Q_{surf} represents surface runoff on day i (mm), E_a represents evapotranspiration on day i (mm), W_{seep} represents water entering the vadose zone from the soil profile on day i (mm), and Q_{gw} represents return flow on day i (mm).

2.7.2. *The Curve of Sediment Rating.* The suspended sediment concentration data collected were insufficient for SWAT model calibration and validation. Unlike streamflow statistics, the Awata station sediment data records obtained from the Ministry of Water, Irrigation, and Electricity show multiple jumps. Because of a lack of continuous-time step suspended sediment recordings, the sediment rating curve for this study was generated by plotting the measured sediment records against the associated streamflow values. The sediment rating curve is a frequently used method for estimating the suspended sediment load carried by a river, linking stream discharge with sediment concentration or load [26].

$$Q_s = 0.0864 * Q_i * C, \quad (4)$$

where Q_s is the sediment load in t/day, Q_i is the instantaneous stream discharge in m³/s, and a and b are regression constants. In this study, a and b were determined to be 8.9676 and 0.9992, respectively, as indicated in Figure 6. The general relationship of the suspended sediment rating curve is shown in equation (5), where Q_s is the sediment load in t/day, Q_i is the stream discharge in m³/s, and a and b are regression constants.

$$Q_s = a * Q_i^b. \quad (5)$$

2.7.3. *Computation of Areal Rainfall.* This study mainly used the Thiessen polygon approach in order to select weather stations contributing to the study area and translate point rainfall values at different stations into an average value since rain gauges only provide point sampling of areal distribution of precipitation, as shown in Figure 7. This technique assumes that rainfall is the same at any place in the watershed as it is at the nearest gauge. Using ArcGIS, the mean areal rainfall

TABLE 4: Land use land cover image classification accuracy assessment report (error matrix).

Class name	Waterbodies	Forest land	Shrubland	Grassland	Built-up area	Agricultural land	Total	Accuracy (%)
Waterbodies	25	0	0	0	0	0	25	100
Forest land	0	24	1	0	0	0	25	96
Shrubland	4	2	47	2	0	2	57	82.46
Grassland	0	0	0	36	0	0	36	100
Built-up area	1	0	0	0	39	1	41	95.12
Agricultural land	1	0	1	6	0	108	116	93.1
Total sampled	31	26	49	44	39	111	300	
Producer's accuracy (%)	80.65	92.31	95.92	81.81	100	97.2		

Overall classification accuracy = 93%. Overall kappa statistics = 0.9.

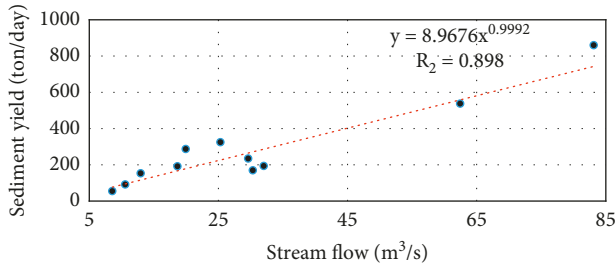


FIGURE 6: Sediment rating curve at the Awata watershed station.

quantity of each station was multiplied by the area of its polygon, and the sum of those products was divided by the total area of the watershed using the following equation:

$$P_{av} = \frac{\sum_{i=1}^n P_i A_i}{\sum_{i=1}^n A_i}, \quad (6)$$

where P_{av} is the average areal rainfall (mm), P_i is the precipitation of stations 1, 2, ..., and A_i is the area coverage of stations 1, 2, ... in the Thiessen polygon. The method gives weight to station data proportion to the space between stations. The area of each polygon inscribed in the watershed, as a percentage of the total subbasin area, was calculated. The sum of the areas of each polygon gives 1912 km², which is equivalent to the total watershed area. The largest and the smallest coverage of the watershed area were represented by Kbremengst and Hagere Selam gauging stations, each covering 36.27% and 3.9%, respectively. Teferekela, Bore, Yirbamuda, and Dilla hold the second, third, fourth, and fifth places in the watershed with areal coverage of 21.48%, 15.76%, 13.47%, and 9.10%, respectively.

2.8. Model Performance, Sensitivity Analysis, Calibration, and Validation. For this study, SWAT CUP-2012 software was utilized to evaluate the SWAT model's performance in estimating sensitivity analysis (parameters), calibration, validation of sediment and streamflow, and uncertainty analysis. Different researchers have used the SUFI-2 algorithm with SWAT CUP for SWAT model performance evaluation, specifically for sediment analysis [26, 27]. This study also applied the SUFI-2 algorithm for streamflow and sediment calibration for its efficiency and quickly applicable to large-scale models where the calibration procedure can take a long time and requires a smaller number of simulations for several basins in arid/semiarid regions like that of the Ganale-Dawa Basin [28]. Using

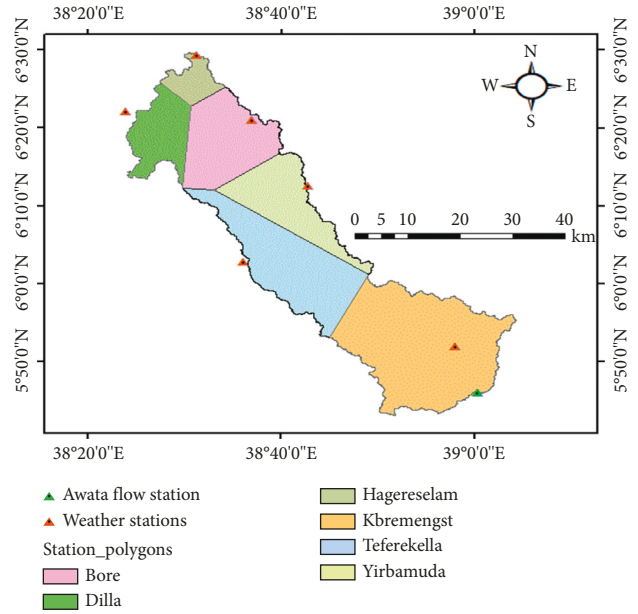


FIGURE 7: Location of gauging stations and Thiessen polygons for weather stations.

a graphical representation of simulated and observed flow or sediment data is a more important strategy for evaluating model performance than statistical measurements. The evaluation of the model was conducted using the following statistical parameters for good fitness of observed data against simulated data:

$$R_2 = \left[\frac{\sum_{i=1}^n (X_{obs} - \bar{X}_{obs})(X_{sim} - \bar{X}_{sim})}{\sqrt{\sum_{i=1}^n (X_{obs} - \bar{X}_{obs})^2 \sum_{i=1}^n (X_{sim} - \bar{X}_{sim})^2}} \right]^2,$$

$$NSE = 1 - \left[\frac{\sum_{i=1}^n (X_{obs} - X_{sim})^2}{\sum_{i=1}^n (X_{obs} - \bar{X}_{obs})^2} \right],$$

$$PBIAS = \left[\frac{\sum_{i=1}^n (X_{obs} - X_{sim})}{\sum_{i=1}^n X_{obs}} \right],$$

$$RSR = \frac{\sqrt{\sum_{i=1}^n (X_{obs} - X_{sim})^2}}{\sqrt{\sum_{i=1}^n (X_{obs} - \bar{X}_{obs})^2}}, \quad (7)$$

where X_{obs} represents observed (measured) values over time, X_{sim} represents simulated values over time, and X_{avs} represents the average of observed and simulated values.

According to [29], uncertainties in SUFI-2 can be measured using the p-factor and r-factor. The p-factor is the percentage of measurable data bracketed by 95PPU (95% prediction uncertainty). The p-factor is an indicator that shows how well all uncertainties are considered. The r-factor is obtained by dividing the average thickness of the 95PPU band by the standard deviation of the measured data. The general methodology used for this study is presented step by step in Figure 8.

2.9. Selected Sediment Reduction Management Scenarios. The SWAT model was used in this work to analyse the effects of four selected management scenarios in the middle Awata watershed. Prioritization of best management practices (BMPs) was involved in these scenarios' analysis, which enables the researcher to make the decision to apply improved management practices. The parameters for these scenarios have been added to the scheduled management operations (ops) input file upon SWAT setup, an optional file that permits the simulation of nonreoccurring management-related activities [30].

2.10. Scenario I: Baseline Conditions. This scenario is the situation with no BMPs and is assumed to reflect the current condition initially executed prior to performing the simulation. In this simulation, the calibrated values of the SWAT model were used without changing any modelling parameters. The baseline scenario is used as a reference for comparisons of the effectiveness of the selected management options and their reduction capacity. The simulated result is used as a point of reference for understanding the effects of simulation results of the following selected sediment reduction options.

2.11. Scenario II: Filter Strips. To decrease the entry of sediment, fertilizers, pesticides, and germs into a surface runoff, filter strips can be put along the edge of the channel [9]. It is a strip of dense vegetation to intercept runoff from upslope pollutant sources and filter it. SWAT provides a specific method to incorporate edge-of-field filter strips through the FILTERS parameter that reflects the width of the strip, which was modified by editing the HRU input table. The effectiveness of the filter strips in the reduction of the sediment yield is based on the trapping efficiency. The trapping efficiency of the strip is a function of its width and is modelled by SWAT. The model can simulate the width of filter strips from 1 m to 30 m based on local research experiences in Ethiopian watersheds [27, 31, 32].

2.12. Scenario III: A Grassed Waterway. By increasing sediment trapping and lowering flow velocity, grassed waterways reduce sediment yield at the channel outlet [23]. For this study, the setup of the grassed waterway was adjusted and simulated with an average width of 3 m and an average depth of 0.141 m, which was $(3/64) * GWATW$ and a 25%

channel slope reduction ($0.75 * HRU\text{-slope}$). The other parameters were automatically adjusted to the default value by the model itself based on the SWAT design specifications [33]. Grassed waterways are installed on gullies and channels for the safe disposal of water into the streams.

2.13. Scenario IV: Contouring. Contouring prevents erosion by slowing down surface runoff and allowing water to penetrate by impounding it in a small depression. This scenario was simulated in SWAT by altering the curve number (CONT_CN) to account for increased surface storage and infiltration and the USLE practice factor (CONT_P) to account for decreased erosion. For this study, CN_II was adjusted by recommendations from the US, SCS (Division, 1986), and CONT_P was adjusted based on literature reports and recommendations available in the SWAT user manual. Contouring was simulated at the critical subbasins for this study by reducing the curve number (CONT_CH) by three units and, based on other literature, adjusting CONT_P to 0.8 depending on the land slope [26, 33, 34].

2.14. Scenario V: Terracing. Application of terracing in a watershed reduces the slope of the HRU and the slope length of the subbasin. Terracing in SWAT is simulated by adjusting both erosion and runoff parameters. The simulation of the effect of terracing on sediment reduction, USLE support practise factor (USLE-P), SCS curve number (CN2), and slope length of the hillside (SLSUBBSN) are the parameters to be adjusted based on the land slope. According to different previous studies, the curve number (TERR_CN) was modified by reducing the value by 10%, which means at least six units [35]. In general, parallel terraces and filter strips can be used to filter the runoff and trap the sediment in a given plot to reduce sediment yield [27]. In general, the performance of those best management practices is calculated by the percentage output of the model using the following equation:

$$\text{the efficiency of BMP} = \frac{\text{PreBMPs} - \text{PostBMPs}}{\text{PreBMPs}} * 100. \quad (8)$$

3. Results and Discussion

3.1. Model Calibration, Validation, and Sensitivity Analysis of Flow Parameters. The flow sensitivity analysis was carried out over an 18-year period, which included two years for the warm-up period (1988–1989) and the next 16-year calibration period (1990–2005). The rank of the parameters was assigned based on the findings of the sensitivity analysis (*t*-stat and *pp* value). The sensitivity analysis was checked for 19 flow parameters using an iteration with 500 simulations, as depicted in Table 5. The analysis result revealed that seven parameters, such as SCS curve number (CN2), average slope steepness (HRU_SLP), maximum canopy index (CANMX), alpha base flow (ALPHA_BF), saturated hydraulic conductivity (SOL_K), and average slope length (SLSUBBSN), had relatively high sensitivity. Five parameters, such as

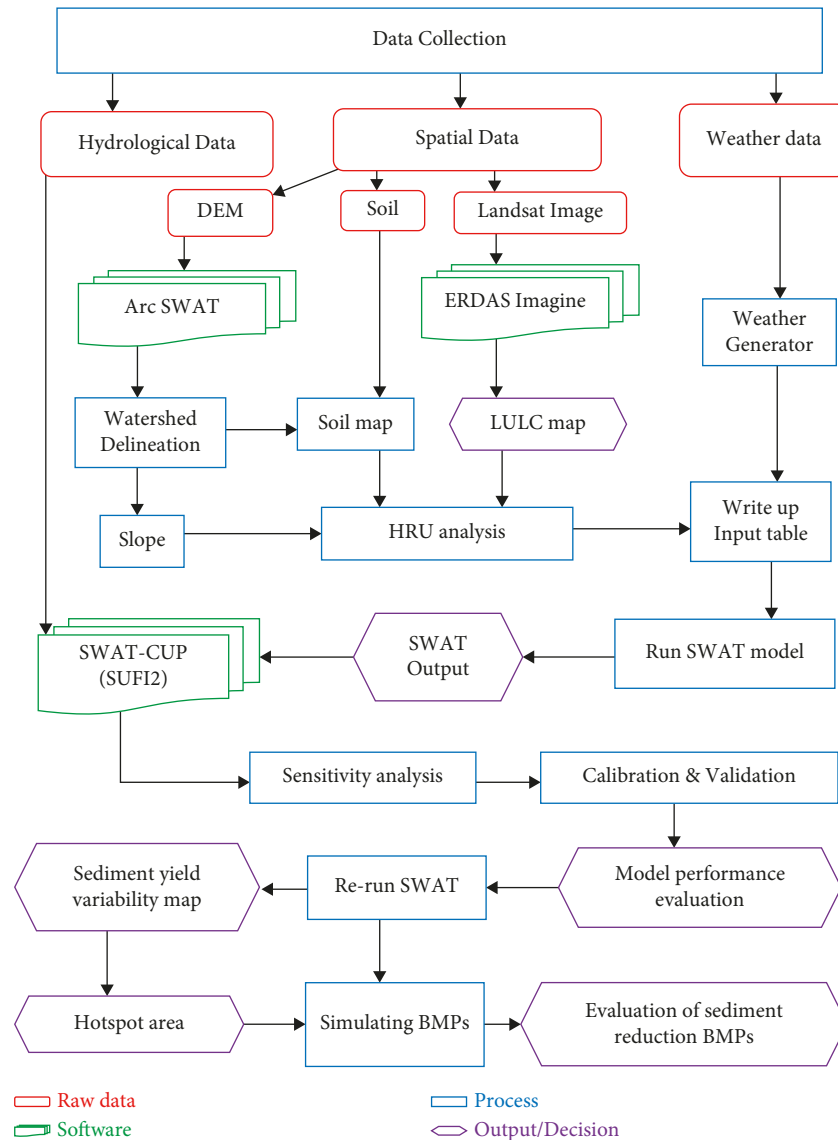


FIGURE 8: General workflow diagram for methodology.

available water content of soil (SOL_AWC), groundwater delay (GW_DELAY), Manning's "n" value for the main channel (CH_N2), effective hydraulic conductivity of main channel alluvium (CH_K2), and surface runoff lag (SUR_LAG), were moderately sensitive. The change in the rest of other parameters was very small or negligible.

3.2. Streamflow Model Calibration. The model calibration is used to decrease uncertainty in the model output and calibrate streamflow on a monthly average basis. The model's performance was evaluated from the initial simulation with parameter values and compared with values for the parameters in the watershed, which showed weak agreement between the simulated and observed streamflow hydrograph. As a result, after identifying the most sensitive parameters, values of selected model parameters were adjusted iteratively within a tolerable range during subsequent calibration until a good agreement between observed and

simulated streamflow was achieved and are presented in Table 6. Calibration and validation of streamflow and sediment yield were carried out at the Awata gauging station with 35 subbasins downstream of the watershed located on the main river course.

The extensions (e.g., hru, mgt, and gw) refer to the SWAT input file where the parameter occurs

The qualifier (V_) refers to the substitution (replace) by a value from the given range

The qualifier (R_) refers to the relative change in the parameter where the value from the SWAT database is multiplied by one plus a factor in the given range

Therefore, high and moderately sensitive twelve parameters were taken as the most influential parameters based on the associated low *pp* value and corresponding high *t*-stat values. The statistical results of the model calibration displayed good performance (R² of 0.76, NSE of 0.75, and

TABLE 5: Summary of calibrated best flow parameters.

No.	Parameter	Description of parameter	Range	Fitted value
1	R_CN2.mgt	SCS runoff curve number	±0.2	0.0097
2	V_HRU_SLP.hru	Average slope steepness	0-1	0.3170
3	V_RCHRG_DP.gw	Deep aquifer percolation fraction	0-1	0.1389
4	V_CANMX.hru	Maximum canopy storage	0-100	0.7525
5	V_ALPHA_BF.gw	Baseflow alpha factor	0-1	0.7273
6	R_SOL_K.sol	Saturated hydraulic conductivity	±0.25	-0.2260
7	R_SLSUBBSN.hru	Average slope length	±0.25	0.1133
8	R_SOL_AWC.sol	Available water content of soil	±0.25	-0.2388
9	V_GW_DELAY.gw	Groundwater delay	100-500	372.77
10	V_CH_N2.rte	“N” value for main channel	-0.01-0.3	0.088
11	V_CH_K2.rte	“K” of main channel alluvium	-0.01-500	260.267
12	V_SURLAG.bsn	Surface runoff lag time	0.05-24	11.55

TABLE 6: Streamflow calibration parameters and their sensitivity rank.

Rank	Parameter	Description of parameter	Range value	t-stat	p value
1	R_CN2.mgt	SCS runoff curve number	±0.2	-16.81	0
2	V_HRU_SLP.hru	Average slope steepness	0-1	-15.94	0
3	V_RCHRG_DP.gw	Deep aquifer percolation fraction	0-1	-15.51	0
4	V_CANMX.hru	Maximum canopy storage	0-100	7.63	0
5	V_ALPHA_BF.gw	Baseflow alpha factor	0-1	6.73	0
6	R_SOL_K.sol	Saturated hydraulic conductivity	±0.25	-5.72	0
7	R_SLSUBBSN.hru	Average slope length	±0.25	4.4	0
8	R_SOL_AWC.sol	Available water content of soil	±0.25	-2.41	0.02
9	V_GW_DELAY.gw	Groundwater delay	100-500	1.38	0.17
10	V_CH_N2.rte	Manning’s “n” value for the main channel	-0.01-0.3	1.25	0.21
11	V_CH_K2.rte	Effective hydraulic conductivity of main channel alluvium	-0.01-500	-0.67	0.5
12	V_SURLAG.bsn	Surface runoff lag time	0.05-24	-0.67	0.5
13	V_GW_REVAP.gw	Groundwater revap coefficient	0.02-0.2	0.52	0.61
14	V_GWQMN.gw	Threshold depth of water in the shallow aquifer for return flow to occur	3500-5000	-0.46	0.65
15	V_REVAPMN.gw	Threshold depth of water in the shallow aquifer for revap to occur	100-500	0.35	0.72
16	V_OV_N.hru	Manning’s “n” value for overland flow	0-1	0.31	0.76
17	V_EPCO.bsn	Plant uptake compensation factor	0-1	0.26	0.79
18	R_SOL_Z.sol	Soil depth (for each layer)	±0.25	-0.1	0.92
19	V_ESCO.bsn	Soil evaporation compensation factor	0-1	-0.06	0.95

PBIAS of +5.6%) between the simulated and observed flow with slight underestimation. The scatter plot of the values of the measured and simulated monthly streamflow data also shows a fair linear correlation between the observed and simulated data as shown in Figure 9.

Validation of the model was carried out using an independent set of measured flow data without further adjustment of the calibrated flow parameter. Hence, statistical analysis for validation results also demonstrated a good agreement between the observed and simulated stream flows with an R2 value of 0.75, NSE of 0.74, and PBIAS of +2.7%, which shows slight underestimation as seen in Figure 10.

The uncertainty measure of SUFI-2 shows a P-factor of 0.60 and an R-factor of 0.75 for calibration and a p-factor of 0.69 and an r-factor of 0.85 for validation at the gauging station, as presented in Table 7. It means that about 60% of the observed data of the calibration and 69% of the observed data of the validation were bracketed by the 95PPU with a better estimation strength while the r-factor was less than one for both cases. This indicates the SWAT model has a low or acceptable level of uncertainty for estimating the

hydrological components and flow of the middle Awata watershed, which is reasonably acceptable for this catchment. The model slightly underestimated and overestimated some of the peaks and low flows. This fluctuation occurred most likely due to the quality of measured weather or/and flow data used as input for the model.

3.3. Modelling of Sediment Yield

3.3.1. Sediment Yield Sensitivity Analysis. Similar procedures to streamflow modelling were followed for sediment modelling. After identifying more sensitive parameters, eleven sediment parameters were examined during the sensitivity analysis of sediment yield, which are USLE_P, USLE_K, LAT_SED, and USLE_C and the next three (SPEXP, CH_EQN, and CH_ERODMO) parameters were determined to be highly and moderately sensitive, respectively, by using *t*-stat and *pp* value. Hence, these parameters have been given high priority for calibration and validation of sediment yield, as depicted in Table 8.

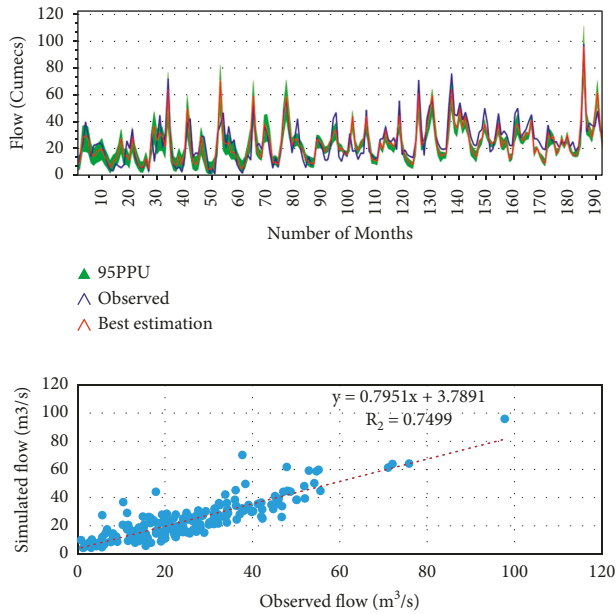


FIGURE 9: Scatter plot and monthly calibrated flow hydrograph at the Awata station.

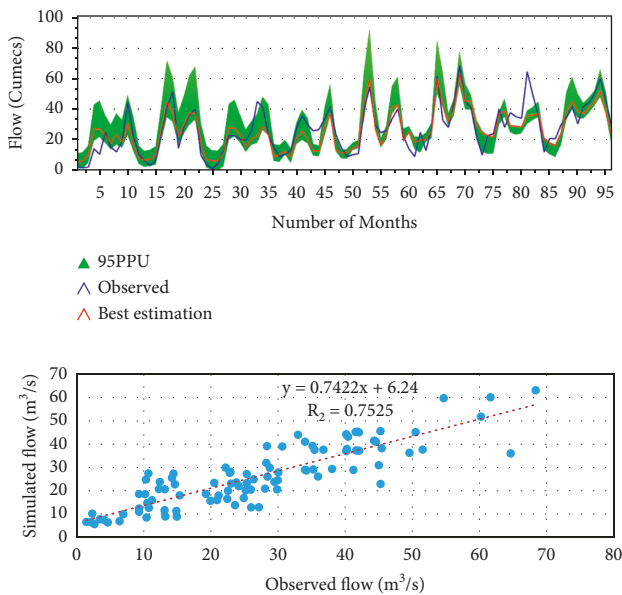


FIGURE 10: Scatter plot and monthly validated flow hydrograph at the Awata station.

3.3.2. Sediment Yield Model Calibration. After identifying sensitive variables, calibrated sediment parameters were developed so that the model could be further used in the watershed being simulated for sediment yield prediction and sediment yield management scenario analysis. After model calibration and validation for streamflow, the model was calibrated and validated for monthly sediment yield at the outlet of Awata gauging station. Similar to flow modelling, the sediment model was calibrated for the period time from 1991 to 2005 as shown in Table 9.

Based on the model performance rating criteria, the monthly basis simulation result for calibration showed good performance with an R^2 of 0.69, an ENS of 0.66, and a PBIAS of 3.7%, as shown in Figure 11. The scatter plot of monthly sediment yield shows a well-fitting relationship between the observed and simulated values for calibration, as indicated in Figure 12.

The performance indicators for the sediment yield validation were within the range of good model estimation performance levels. The scatter plot of the values of the observed and simulated monthly sediment yield data also shows a fair linear correlation between the two datasets for the validation period shown in Figure 13. The ability of models in sediment yield estimation and their prediction uncertainty for validation were checked through the statistical performance indicators. The results showed an R^2 of 0.67, an ENS of 0.65, and a PBIAS of 5.6%, which shows good fitness, as shown in Figure 14.

In general, the uncertainty measured by SUFI-2 with 58% observed sediment yield on monthly data at Awata station was bracketed by the 95PPU for calibration with a better strength of estimation in which r -factor < 1 and the validation period was also within the acceptable range of model uncertainty. This result is shown in Table 10 with different parameters that estimate the percentage of uncertainty with the model. Although the model slightly underestimated the basin's sediment supply by 3.7% for calibration and 5.6% for validation at the outlet, the statistical model performance indicators showed that the model performed well and it is acceptable.

3.4. Sediment Yield Spatial Variability. The spatial variability of sediment yield in the catchments was significant in identifying the soil erosion prone area in the middle of the Awata watershed that was most in need of sediment reduction management planning. Rerunning the model with fitted values of all flow and sediment calibration parameters for 1988–2018 generated the average yearly sediment yield at subbasin level for the entire watershed region. As a result, the sediment outflow rate from each tributary and main river segment was calculated. The simulated annual sediment yield rate was used to determine the spatial variability for the entire watershed, ranging from 3.49 to 40.99 t/ha/year with an average of 13.67 t/ha/year at the subbasin level, as seen in Table 11.

Because of the combined effect of land use land cover, soil type, slope, weather conditions, and runoff conditions, sediment yields from each subbasin varied. Thus, the sediment yield spatial variability map in the watershed was obtained by using the annual sediment yield rate from each subbasin area to indicate the most severe subbasin due to erosion severity classes. The severity of soil erosion in the catchment suggests a deliberate response to the highly prone areas of subbasins for sediment reduction management, which was also concluded by the authors of [27] with investigations made into other watershed regions in Ethiopia. It also plays a critical function in raising awareness about watershed status in terms of soil erosion and response to the prone area. The spatial map of sediment yield variability at a subbasin scale for the entire

TABLE 7: General statistics of streamflow calibration and validation.

Simulation period	Uncertainty measures		Model performance indicators			
	p-factor	r-factor	R2	NSE	RSR	PBIAS (%)
Calibration (1990–2005)	0.6	0.75	0.76	0.75	0.51	+5.6
Validation (2006–2013)	0.7	0.8	0.75	0.74	0.5	+2.7

TABLE 8: Sediment calibration parameters and their sensitivity ranks.

Rank	Parameter name	Description of parameter	Range	t-stat	p value
1	USLE_P.mgt	USLE support practice factor	0–0.6	–6.54	0
2	USLE_K.sol	USLE soil erodibility factor	0–0.1	–5.99	0
3	LAT_SED.hru	Sediment intensity in LAT and GW	0–120	5.77	0
4	USLE_C.plant.dat	USLE land cover management factor	0–0.5	–3.34	0.001
5	SPEXP.bsn	Re-entrained channel sediment routing	1–2	–1.28	0.20
6	CH_EQN.rte	Sediment routing method	0–0.001	–1.12	0.26
7	CH_ERODMO	Channel erodibility factor	0–1	1.11	0.27
8	CH_COV1.rte	Channel erodibility factor	0.6–1	–0.24	0.82
9	BIOMIX.mgt	Biological mixing efficiency	0–1	–0.22	0.83
10	CH_COV2.rte	Channel cover factor	0.6–1	0.08	0.93
11	SPCON.bsn	Parameter for channel sediment routing	0–0.01	–0.02	0.99

TABLE 9: Summary of sediment calibrated parameter values for the study area.

No.	Parameter	Description of parameter	Range value	Calibrated value
1	USLE_P.mgt	USLE support practice factor	0–0.6	0.546
2	USLE_K.sol	USLE soil erodibility factor	0–0.1	0.012
3	LAT_SED.hru	Sediment concentration in lateral and groundwater flow	0–120	117.95
4	USLE_C.plant.dat	Universal soil loss equation land cover management factor	0.003–0.5	0.144
5	SPEXP.bsn	Parameter for calculating sediment re-entrained in channel sediment routing	1–2	1.61
6	CH_EQN.rte	Sediment routing method	0–0.001	0.00033
7	CH_ERODMO.rte	Channel erodibility factor	0–1	0.69

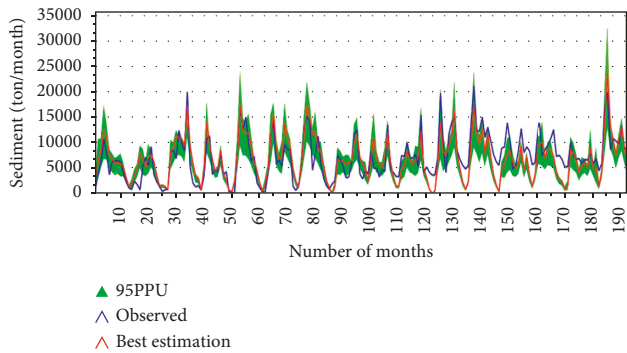


FIGURE 11: Monthly calibrated sediment yield hydrograph at the Awata station.

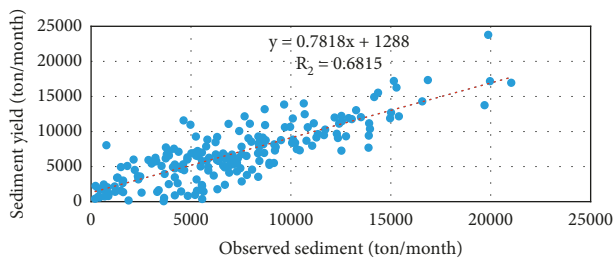


FIGURE 12: Scatter plot of simulated and observed sediment yield for calibration (1990–2005).

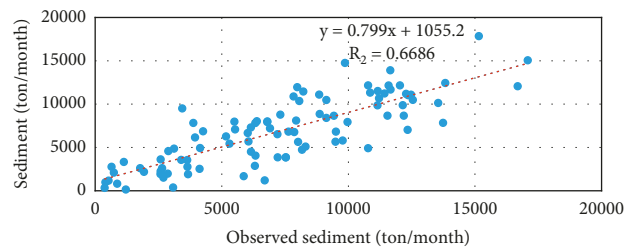


FIGURE 13: Scatter plot of sediment yield for the validation period (2006–2013).

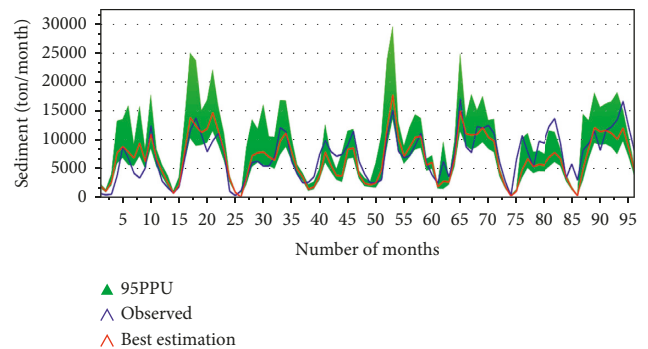


FIGURE 14: Monthly validated sediment yield hydrograph at the Awata station.

TABLE 10: General sediment calibration and validation statistics.

Simulation period	Uncertainty measures		Model performance indicators			
	p-factor	r-factor	R2	NSE	RSR	PBIAS (%)
Calibration (1990–2005)	0.58	0.91	0.69	0.66	0.58	+3.7
Validation (2006–2013)	0.64	0.61	0.67	0.65	0.61	+5.6

TABLE 11: The simulated sediment yield of the middle Awata watershed subbasins.

Subbasin	Area (km ²)	Sed. yield (t/ha)	Subbasin	Area (km ²)	Sed. yield (t/ha)
1	48.20	19.72	20	30.91	8.38
2	10.42	33.18	21	181.39	5.76
3	106.42	23.52	22	102.34	3.49
4	4.77	33.49	23	29.79	5.46
5	28.23	40.99	24	5.52	5.58
6	60.36	15.80	25	115.57	4.55
7	46.42	16.81	26	37.55	8.29
8	38.86	19.77	27	92.83	6.00
9	57.73	28.20	28	28.21	8.26
10	33.67	40.55	29	99.41	8.84
11	41.36	30.46	30	34.13	9.02
12	30.06	31.66	31	108.77	6.78
13	29.36	7.33	32	66.66	6.69
14	78.71	6.34	33	50.72	6.07
15	22.40	7.64	34	55.76	8.28
16	27.52	6.62	35	10.50	9.69
17	63.47	9.56	36	40.25	4.83
18	8.44	5.17	37	54.56	7.87
19	30.64	4.98			

middle Awata watershed concluded that there were high-prone areas. Based on soil loss severity class, six subbasins were designated as severely affected areas, two subbasins were very highly affected areas, four subbasins were highly affected areas, twenty subbasins were moderately affected, and the remaining four subbasins were low erosion-prone areas that were exposed to sedimentation as seen on the sediment yield spatial variability map (Figure 15). The upstream subbasins contribute the majority of the annual sediment yield due to their dominant sediment yield rate compared to subbasins towards the outlet of the watershed. Thus, the subbasins in the northern part of the watershed were identified as soil erosion hot spot (prone) areas.

This study identified the middle Awata watershed sediment severity classes from high to severe, in which the first twelve subbasins having an average annual sediment load ranging from 11 to 41 t/ha/year were identified as soil erosion vulnerable areas. The soil erosion for the hot spot area was 506.5 km², which covers about 26.49% of the total watershed area. These soil erosion critical subwatersheds are dominantly covered with agricultural areas, pastures, and shrubland with steeper mean average slopes, as shown in Table 12. Chluvisol and vertisol soil types were justified as the main causes of annual sediment yield to the watershed.

3.5. Analysis of Sediment Reduction Management Scenarios

3.5.1. Baseline Scenario. According to the sediment load output obtained from SWAT output, the average annual sediment loading was spatially varied, and at the entire

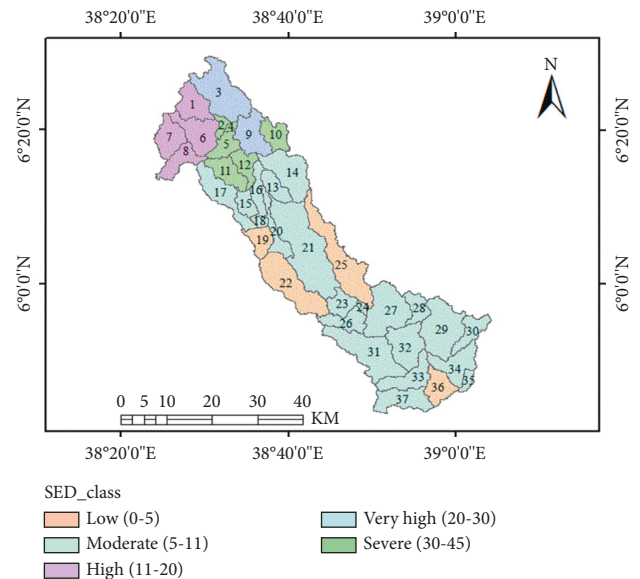


FIGURE 15: Spatial variability map of sediment yield in the middle Awata watershed.

watershed, the reach outlet was 13.67 t/ha/year and 34.543×103 ton/year, respectively (reach number 35 in Appendix-H). The sediment yield for each of the 12 identified critical subbasins was indicated in Table 12, and from the selected hot spot subbasins, six were identified as severely affected areas with erosion potential (30–45 t/ha/year), two subbasins as very highly affected areas (20–30 t/ha/year), and four subbasins as highly affected (11–20 t/ha/year). These

TABLE 12: Soil erosion prone at subbasins' level with their dominant LULC, soil type, and average slope.

Critical subbasin	Subbasin area (km ²)	Covered area (km ²)	SWAT dominant LULC		SWAT dominant soil class		Mean slope (%)	SED yield (t/ha/year)
			Major LULC	Coverage (%)	Soil type	Coverage (%)		
1	48.204	44.99	AGRL, PAST, SHRB	93.34	Chluvisols, euvertisols	100	17.74	19.72
2	10.415	10.27	AGRL, PAST, SHRB	98.64	Chluvisols	100	16.76	33.18
3	106.42	102.51	AGRL, PAST, SHRB	96.33	Chluvisols, euvertisols	100	16.94	23.52
4	4.7742	4.57	AGRL, PAST, SHRB	95.62	Chluvisols	100	16.47	33.49
5	28.227	27.50	AGRL, PAST, SHRB	97.44	Chluvisols	100	18.14	40.99
6	60.358	58.90	AGRL, PAST, SHRB	97.59	Chluvisols, euvertisols	100	16.94	15.80
7	46.422	36.85	AGRL, PAST, SHRB	79.38	Chluvisols, euvertisols	100	18.70	16.81
8	38.859	35.35	AGRL, PAST, SHRB	90.97	Chluvisols	100	18.73	19.77
9	57.734	54.89	AGRL, PAST, SHRB	95.08	Chluvisols, euvertisols	100	22.52	28.20
10	33.665	31.97	AGRL, PAST, SHRB	94.97	Chluvisols, euvertisols	100	20.90	40.55
11	41.356	39.80	AGRL, PAST, SHRB	96.24	Chluvisols	100	18.79	30.46
12	30.056	28.56	AGRL, PAST, SHRB	95.04	Chluvisols	100	18.95	31.66

critical subbasins cover about 26.5% of the total watershed area, with an average sediment yield contribution of 27.85 t/ha/year as presented in Figure 16. By applying best management practices to these prone areas of sedimentation, the results were compared with this baseline condition to apply best sediment management practices.

3.5.2. Applying Filter Strips (FS) (Scenario I). As shown in Table 13, the application of 1 m filter strips reduced the average annual sediment yield for critical subbasins from 27.85 t/ha/year to 22.98 t/ha/year, with an average of 17.48% reduction capacity. The study conducted by the authors of [27] indicated the implementation of 1 m wide filter strips for critical subbasins and reported a 13.7% mean annual sediment yield reduction for the critical subbasins from the baseline scenario.

3.5.3. Using a Grassy Waterway (Scenario II). After simulation of grassed waterways with an average width of 3 m for the selected critical source subbasins, 38.18% of the average sediment yield has been reduced from 27.85 t/ha/year to 17.21 t/ha/year, as shown in Table 14. For the entire watershed, the mean annual sediment yield decreased by 25.23% (from 13.67 t/ha/year to 10.217 t/ha/year). The grassed waterway is effective for sediment reduction since it can trap the silt generated from the erosion field and reduce the development of channel erosion. The study conducted by the authors of [36] also proved that the application of grassed waterways reduced the average sediment yield by 53%.

3.5.4. Applying Contouring (Scenario III). This practice reduced the sediment yield rate from an average annual sediment yield of 27.85 t/ha/year to 18.54 t/ha/year, a 33.43% reduction as shown in Table 15. Installing contours on agricultural land, shrubland, and pastures increases infiltration by increasing surface roughness. This, in turn, reduces the speed and erosion power of runoff. At the watershed level, the average annual baseline sediment yield of 13.67 t/ha/year was reduced by 22.09% to 10.65 t/ha/year. Another study [34] has studied the effectiveness of contour farming and filter strips on ecosystem services and found that about 35.8% of the average annual sediment yield is reduced by contour farming. Also, the study [37] has found that about 22% of the sediment yield is reduced by the application of contour farming in order to overcome land degradation problems. Hence, the result of this study has slightly agreed with those studies so far.

3.5.5. Applying Parallel Terracing. Implementing terraces in the selected critical subbasins reduced the mean annual sediment yield rate by 47.05%. As shown in Table 16, which shows the effect of terracing on each critical area, the average sediment yield rate of the subbasins was significantly reduced from 27.85 t/ha/year to 14.74 t/ha/year.

At the whole watershed level, the model output also showed that annual sediment yield was reduced by 30.09% from an average yield of 13.67 t/ha/year to 9.42 t/ha/year after applying terraces on critical subbasins. The study by [20] found that applying terracing in the Guder watershed, Blue Nile Basin, reduced the average annual sediment yield by 53% from the baseline scenario at selected subbasin areas.

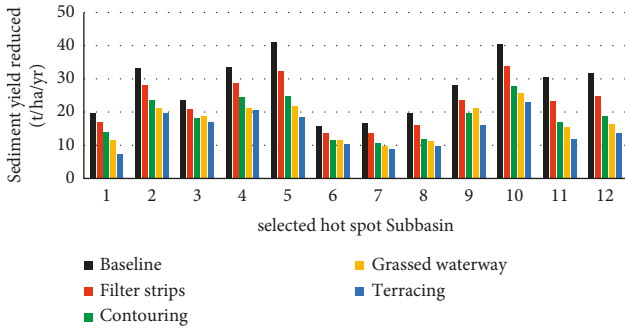


FIGURE 16: Comparison of sediment reduction by selected BMPs at critical subbasins.

TABLE 13: Sediment reduction with filter strip simulation.

Hot spot subbasin	Average annual sediment loading (t/ha/year)		Reduction (%)
	Baseline	After FS (1 m)	
1	19.72	16.90	14.31
2	33.18	28.01	15.59
3	23.52	21.00	10.69
4	33.49	28.61	14.56
5	40.99	32.41	20.93
6	15.80	13.69	13.33
7	16.81	13.78	18.04
8	19.77	15.94	19.36
9	28.20	23.57	16.41
10	40.55	33.78	16.71
11	30.46	23.31	23.46
12	31.66	24.79	21.69

TABLE 14: Sediment reduction using grassed waterway simulation.

Hot spot subbasin	Average annual sediment loading (t/ha/year)		Reduction (%)
	Baseline	After GWAT	
1	19.72	11.53	41.56
2	33.18	21.12	36.35
3	23.52	18.86	19.81
4	33.49	21.36	36.22
5	40.99	21.82	46.75
6	15.80	11.70	25.96
7	16.81	9.83	41.51
8	19.77	11.37	42.48
9	28.20	21.36	24.25
10	40.55	25.86	36.23
11	30.46	15.43	49.35
12	31.66	16.32	48.44

3.6. Evaluation of Best Management Practices. In general, the study investigates that allowing filter strips with a 1-metre strip width has the least sediment reduction capability at all critical subbasins of the watershed, which reduced only about 17.46% of the mean annual sediment load. The application of 1 m wide filter strips reduced the total watershed sediment yield by 11.54% (13.67 t/ha/year to 12.09 t/ha/year). This scenario has shown more consistent reduction

TABLE 15: Summary of sediment reduction with contouring simulation.

Hot spot subbasin	Average annual sediment loading (t/ha/year)		Reduction (%)
	Baseline	After contouring	
1	19.72	13.94	29.32
2	33.18	23.55	29.04
3	23.52	18.32	22.12
4	33.49	24.40	27.14
5	40.99	24.89	39.26
6	15.80	11.52	27.10
7	16.81	10.56	37.16
8	19.77	11.88	39.90
9	28.20	19.60	30.49
10	40.55	27.86	31.29
11	30.46	17.10	43.84
12	31.66	18.83	40.53

TABLE 16: Summary of sediment reduction with the simulation of terracing.

Hot spot subbasin	Average annual sediment loading (t/ha/year)		Reduction (%)
	Baseline	After terracing	
1	19.72	7.24	63.30
2	33.18	19.68	40.70
3	23.52	16.92	28.07
4	33.49	20.75	38.03
5	40.99	18.57	54.69
6	15.80	10.37	34.37
7	16.81	8.91	47.01
8	19.77	9.80	50.43
9	28.20	16.20	42.54
10	40.55	22.86	43.63
11	30.46	11.85	61.10
12	31.66	13.77	56.50

TABLE 17: Sediment yield reduction effectiveness and rank of BMPs on Awata watersheds.

Rank	Types of BMP	SED yield before BMP (t/ha/year)	SED yield after BMP (t/ha/year)	Reduction (%)
1	Terracing	27.85	14.74	47.05
2	Grassed waterway	27.85	17.21	38.18
3	Contouring	27.85	18.54	33.43
4	Filter strips	27.85	22.98	17.48

characteristics than the others, even though it is the least effective. Next to filter strips, the average reduction effectiveness of contouring for critical subbasins was 33.43%, which was relatively higher than filter strips but lower than grassed waterways (38.18%) and terracing (47.05%). The highest reduction of contouring was observed at subbasins 11 and 12, which were reduced by 43.84% and 40.53%, respectively. This was a better reduction than what filter strips could do in the same subbasin area. The percentage of

sediment reduction in each BMP was calculated as described in Table 17. Grassed waterways have put themselves in the second sediment reduction effectiveness rank, next to terracing, in most subbasins. It reduced 38.18% of the critical subbasins' annual sediment yield rate from 27.85 t/ha/year to 17.21 t/ha/yr. Furthermore, terracing resulted in the greatest relative sediment reduction across all critical subbasins. It has shown relatively consistent spatial variability, varying between 28.07% at subbasin-3 and 63.30% at subbasin-1, with average reduction effectiveness of 47.05%. Generally, the analysis has observed that terracing was more effective than other management practices at all hotspots in this watershed region.

4. Conclusion

Sediment yields from soil erosion and sediment accumulation have a significant impact on water resource development planning. The issue of sedimentation poses a dangerous obstacle in the design, planning, and management of river basin water resources' projects unless the upstream is handled with effective watershed management practices. This study used the SWAT model for sediment yield for simulation of the middle Awata watershed. The SWAT model was then calibrated from 1990 to 2005 and validated from 2006 to 2013 every month using observed values to examine its applicability for simulation of streamflow and sediment yield using the SUFI-2 algorithm in SWAT_CUP. The statistical results of model calibration and validation displayed very good performance with $R^2 = 0.76$, $NSE = 0.75$, $RSR = 0.51$, and $PBIAS = 5.6\%$ and $R^2 = 0.75$, $NSE = 0.74$, $RSR = 0.51$, and $PBIAS = 2.7\%$, respectively, for streamflow, while the simulation results for calibration and validation of sediment yield have shown good model performance rates with $R^2 = 0.69$, $ENS = 0.66$, $RSR = 0.58$, and $PBIAS = 3.7\%$ and $R^2 = 0.67$, $ENS = 0.65$, $RSR = 0.61$, and $PBIAS = 5.6\%$, respectively. The SWAT model simulation for existing conditions predicted sediment yield at the watershed outlet to be 34.543×10^3 ton/year with an average spatial distribution of 13.67 t/ha/year for the given simulation period. The first 12 upstream subbasins (about 26.49% of the total watershed area) with an average annual sediment load of 11–41 t/ha/year were identified as soil erosion vulnerable areas. The SWAT model was applied to simulate the effects of four selected sediment yield reduction best management practises scenarios. The simulation results showed that installing a filter strip, contouring, grassed waterway, and parallel terracing on the critical subbasins reduced sediment yield by 17.46%, 33.43%, 38.18%, and 47.05%, respectively. As a result, terracing was the most effective sediment reduction option in landuse, slope, and soil conditions for almost all critical subbasins.

Data Availability

All data are included in the article, and if needed, they will be submitted upon request.

Conflicts of Interest

The authors declare no conflicts of interest.

Acknowledgments

The authors would like to thank the Ethiopian meteorological agency and the Ministry of Water, Irrigation, and Electricity for their great willingness in giving necessary data for the accomplishments of this research.

References

- [1] D. N. Khoi and T. Suetsugi, "The responses of hydrological processes and sediment yield to land-use and climate change in the be River catchment, Vietnam," *Hydrological Processes*, vol. 28, no. 3, pp. 640–652, 2014.
- [2] W. T. Dibaba, T. A. Demissie, and K. Miegel, "Drivers and implications of land use/land cover dynamics in Finchaa catchment, Northwestern Ethiopia," *Land*, vol. 9, no. 4, pp. 113–122, 2020.
- [3] X. Yang, B. Guo, Y. Lu et al., "Spatial-temporal evolution patterns of soil erosion in the Yellow River Basin from 1990 to 2015: impacts of natural factors and land use change," *Geomatics, Natural Hazards and Risk*, vol. 12, no. 1, pp. 103–122, 2021.
- [4] J. Hirschberg, S. Fatichi, G. L. Bennett et al., "Climate change impacts on sediment yield and debris-flow activity in an alpine catchment," *Journal of Geophysical Research: Earth Surface*, vol. 126, no. 1, pp. 1–34, 2021.
- [5] M. Hajigholizadeh, A. Melesse, and H. Fuentes, "Erosion and sediment transport modelling in shallow waters: a review on approaches, models and applications," *International Journal of Environmental Research and Public Health*, vol. 15, no. 3, p. 518, 2018.
- [6] B. Ambade, A. Kumar, A. Kumar, and L. K. Sahu, "Temporal variability of atmospheric particulate-bound polycyclic aromatic hydrocarbons (PAHs) over central East India: sources and carcinogenic risk assessment," *Air Quality, Atmosphere & Health*, vol. 15, no. 1, pp. 115–130, 2022.
- [7] M. A. Parsons, J. C. Lewis, J. N. Pauli et al., "Prey of reintroduced fishers and their habitat relationships in the cascades range, Washington," *Forest Ecology and Management*, vol. 460, Article ID 117888, 2020.
- [8] B. Ambade and S. S. Sethi, "Health risk assessment and characterization of polycyclic aromatic hydrocarbon from the hydrosphere," *Journal of Hazardous, Toxic, and Radioactive Waste*, vol. 25, no. 2, pp. 1–11, 2021.
- [9] M. L. Berihun, A. Tsunekawa, N. Haregeweyn et al., "Evaluating runoff and sediment responses to soil and water conservation practices by employing alternative modeling approaches," *The Science of the Total Environment*, vol. 747, Article ID 141118, 2020.
- [10] M. Kidane, A. Bezie, N. Kesete, and T. Tolessa, "The impact of land use and land cover (LULC) dynamics on soil erosion and sediment yield in Ethiopia," *Heliyon*, vol. 5, no. 12, Article ID e02981, 2019.
- [11] C. D. Guzman, S. A. Tilahun, A. D. Zegeye, and T. S. Steenhuis, "Suspended sediment concentration-discharge relationships in the (sub-) humid Ethiopian highlands," *Hydrology and Earth System Sciences*, vol. 17, no. 3, pp. 1067–1077, 2013.
- [12] M. Mohammadi, A. Khaledi Darvishan, V. Spalevic, B. Dudic, and P. Billi, "Analysis of the impact of land use changes on soil

- erosion intensity and sediment yield using the intero model in the talar watershed of Iran,” *Water*, vol. 13, no. 6, pp. 881–915, 2021.
- [13] S. Kurwadkar, J. Dane, S. R. Kanel et al., “Per- and poly-fluoroalkyl substances in water and wastewater: a critical review of their global occurrence and distribution,” *The Science of the Total Environment*, vol. 809, Article ID 151003, 2022.
- [14] I. A. Kuti and T. A. Ewemoje, “Modelling of sediment yield using the soil and water assessment tool (SWAT) model: a case study of the Chanchaga Watersheds, Nigeria,” *Scientific African*, vol. 13, Article ID e00936, 2021.
- [15] A. Maqsoom, B. Aslam, U. Hassan et al., “Geospatial assessment of soil erosion intensity and sediment yield using the Revised Universal Soil Loss Equation (RUSLE) model,” *ISPRS International Journal of Geo-Information*, vol. 9, no. 6, pp. 356–6, 2020.
- [16] J.-G. Wang, B. Yu, S.-M. Ni, Z.-L. Guo, and C.-F. Cai, “Effects of sediment load on the abrasion of soil aggregate and hydraulic parameters in experimental overland flow,” *Journal of Integrative Agriculture*, vol. 19, no. 4, pp. 1117–1126, 2020.
- [17] C. Tundu, M. J. Tumbare, and J.-M. Kileshye Onema, “Sedimentation and its impacts/effects on river system and reservoir water quality: case study of Mazowe catchment, Zimbabwe,” *Proceedings of the International Association of Hydrological Sciences*, vol. 377, pp. 57–66, 2018.
- [18] B. Ambade, T. K. Sankar, A. S. Panicker, A. S. Gautam, and S. Gautam, “Characterization, seasonal variation, source apportionment and health risk assessment of black carbon over an urban region of East India,” *Urban Climate*, vol. 38, Article ID 100896, 2021.
- [19] B. Berhanu, Y. Seleshi, M. Amare, and A. M. Melesse, *Upstream–Downstream Linkages of Hydrological Processes in the Nile River Basin*, Springer Geography, Berlin, Germany, 2016.
- [20] B. Nadew’, E. Chaniyalew, and T. Tsegaye, “Runoff sediment yield modeling and development of management intervention scenarios, case study of guder watershed, Blue Nile Basin, Ethiopia,” *Hydrology: Current Research*, vol. 9, no. 4, pp. 0–16, 2019.
- [21] N. Zalaki-badil, S. Eslamian, G. Sayyad, and S. Hosseini, “Using SWAT model to determine runoff, sediment yield in maroon-dam catchment,” *International Journal of Research Studies in Agricultural Sciences*, vol. 3, no. 12, pp. 31–41, 2017.
- [22] A. B. Ayana, D. C. Edossa, and E. Kositsakulchai, “Simulation of sediment yield using SWAT model in Fincha Watershed, Ethiopia,” *Kasetsart Journal*, vol. 46, no. 2, pp. 283–297, 2012.
- [23] D. Husen and B. Abate, “Estimation of runoff and sediment yield using SWAT model: the case of katar watershed, Rift Valley Lake basin of Ethiopia,” *International Journal of Mechanical Engineering and Applications*, vol. 8, no. 6, p. 125, 2020.
- [24] M. G. Ali, S. Ali, R. H. Arshad et al., “Estimation of potential soil erosion and sediment yield: a case study of the trans-boundary chenab river catchment,” *Water*, vol. 13, no. 24, pp. 3647–3723, 2021.
- [25] M. F. Baig, M. R. U. Mustafa, I. Baig, H. B. Takaijudin, and M. T. Zeshan, “Assessment of land use land cover changes and future predictions using CA-ANN simulation for selangor, Malaysia,” *Water*, vol. 14, no. 3, p. 402, 2022.
- [26] W. T. Dibaba, T. A. Demissie, and K. Miegel, “Prioritization of sub-watersheds to sediment yield and evaluation of best management practices in highland Ethiopia, finchaa catchment,” *Land*, vol. 10, no. 6, p. 650, 2021.
- [27] T. Gashaw, Y. T. Dile, A. W. Worqlul et al., “Evaluating the effectiveness of best management practices on soil erosion reduction using the SWAT model: for the case of gumara watershed, abbay (upper Blue Nile) Basin,” *Environmental Management*, vol. 68, no. 2, pp. 240–261, 2021.
- [28] S. H. Hosseini and M. R. Khaleghi, “Application of SWAT model and SWAT-CUP software in simulation and analysis of sediment uncertainty in arid and semi-arid watersheds (case study: the Zoshk-Abardeh watershed),” *Modeling Earth Systems and Environment*, vol. 6, no. 4, pp. 2003–2013, 2020.
- [29] B. Narsimlu, A. K. Gosain, B. R. Chahar, S. K. Singh, and P. K. Srivastava, “SWAT model calibration and uncertainty analysis for streamflow prediction in the kunwari River Basin, India, using sequential uncertainty fitting,” *Environmental Processes*, vol. 2, no. 1, 2015.
- [30] G. Nabi, F. Hussain, R.-S. Wu, V. Nangia, and R. Bibi, “Micro-watershed management for erosion control using soil and water conservation structures and SWAT modeling,” *Water*, vol. 12, no. 5, pp. 1439–1525, 2020.
- [31] H. Lemma, A. Frankl, A. Griensven, J. Poesen, E. Adgo, and J. Nyssen, “Identifying erosion hotspots in lake tana basin from a multisite soil and water assessment tool validation: opportunity for land managers,” *Land Degradation & Development*, vol. 30, no. 12, pp. 1449–1467, 2019.
- [32] F.-Z. Lee, J.-S. Lai, and T. Sumi, “Reservoir sediment management and downstream river impacts for sustainable water resources-case study of shihmen reservoir,” *Water*, vol. 14, no. 3, p. 479, 2022.
- [33] Y. Liu, T. Guo, R. Wang et al., “A SWAT-based optimization tool for obtaining cost-effective strategies for agricultural conservation practice implementation at watershed scales,” *The Science of the Total Environment*, vol. 691, pp. 685–696, 2019.
- [34] J. Gathagu, K. Mourad, and J. Sang, “Effectiveness of contour farming and filter strips on ecosystem services,” *Water*, vol. 10, no. 10, pp. 1312–10, 2018.
- [35] M. L. Berihun, A. Tsunekawa, N. Haregeweyn et al., “Reduced runoff and sediment loss under alternative land capability-based land use and management options in a sub-humid watershed of Ethiopia,” *Journal of Hydrology: Regional Studies*, vol. 40, Article ID 100998, 2022.
- [36] J. Sun, C.-H. Huang, G. Han, and Y. Wang, “Effects of cover on soil particle and associated soil nutrient redistribution on slopes under rainfall simulation,” *Journal of Soils and Sediments*, vol. 19, no. 2, pp. 729–740, 2019.
- [37] G. F. Ricci, J. Jeong, A. M. De Girolamo, and F. Gentile, “Effectiveness and feasibility of different management practices to reduce soil erosion in an agricultural watershed,” *Land Use Policy*, vol. 90, Article ID 104306, 2020.